Thin Solid Films 763 (2022) 139560

Contents lists available at ScienceDirect

Thin Solid Films

journal homepage: www.elsevier.com/locate/tsf

Crosspolarization with imperfect infrared polarizers

Andreas Furchner [a,*], Karsten Hinrichs [b]

[a] Helmholtz-Zentrum Berlin für Materialien und Energie GmbH, Division Energy and Information, Schwarzschildstraße 8, 12489 Berlin, Germany
[b] Leibniz-Institut für Analytische Wissenschaften – ISAS – e. V., Schwarzschildstraße 8, 12489 Berlin, Germany

ARTICLE INFO

Keywords:
Infrared polarimetry
Infrared spectroscopy
Polarizer leakage
Imperfect polarizers
Analysis of infrared bands
Weak anisotropy
Crosspolarization

ABSTRACT

The analysis of vibrational bands is a core application of infrared (IR) spectroscopy. Polarization-dependent measurements enable the study of anisotropic materials. However, imperfect IR polarizers exhibit polarizer leakage, which causes pronounced bandshape and baseline distortions for samples with weak optical anisotropy. Based on the 4 × 4 Mueller-matrix formalism, we propose a polarimetric measurement scheme for handling imperfect polarizers and source prepolarization that delivers correct co- and crosspolarized transmission and reflection IR spectra. The scheme is applied to a weakly anisotropic polypropylene sheet, resolving crosspolarized signatures as small as $5 \cdot 10^{-5}$. We determine the polymer's direction-dependent complex refractive index in the vibrational fingerprint range.

1. Introduction

The anisotropy of a material's optical, mechanical, physical and chemical properties plays a key role in optoelectronic, photonic, polymer, catalytic and biorelated research and applications [1–3]. Label-free optical methods that work with polarized light are particularly attractive for analyzing structural, functional, electronic and optical anisotropy as they can measure polarization-dependent material characteristics in a contactless manner [4–14].

Direct identification of anisotropies is possible by means of spectroscopic and microscopic techniques that measure crosspolarized optical signals. Such spectroscopies are well-established in the visible to near-infrared spectral range for imaging in biology, material science, photonics and mineralogy [5–17]. For example, crosspolarized measurements are used in optical coherence tomography of tissues as a tool to increase the optical contrast [6–8], in microscopic imaging of biological [14] and mineral [9] samples, in reflectance measurements of teeth [11], in polarized photoluminescence excitation spectroscopy of carbon nanotubes [13], in scanning near-field optical microscopy of metallic gratings [15] and plasmonic structures [10], and in ellipsometry of beetle cuticles [18] and ordered nanostructures [19].

It is also known for the infrared (IR) spectral range that crosspolarized spectroscopic measurements can improve the analysis of anisotropic and heterogeneous materials. Crosspolarized IR-spectroscopic measurements have been discussed for decades in several ellipsometric applications [16,17,20–22] and applied, for instance, for detailed studies of metamaterials [16] and their use in enhancing the vibrational contrast of molecular monolayers [17].

Recently, crosspolarized IR-polarimetric measurements served as a quick identifier of anisotropies of aligned nanofibers used as substrates for nerve-tissue regeneration [12]. Although the detected crosspolarized signals were small, the specific orientation of molecular vibrations, and the corresponding anisotropic and isotropic optical behavior, could be directly identified in sample measurements under different azimuthal rotations.

However, a systematic analysis of weakly anisotropic spectral band contributions has not been performed yet for crosspolarized mid-IR spectra in the so-called fingerprint region. One challenge here is that mid-IR wire-grid polarizers are imperfect optical elements, in that they leak a small but significant portion of orthogonally-polarized light with respect to their principal polarization direction. Such leakage needs to be considered for quantitative interpretation [23]. Examples in the literature so far only discuss copolarized measurements and how these are influenced by potential effects from polarizer leakage [23,24]. These previous studies aimed to measure "cross-contaminated" reflectances and to retrospectively account for said leakage by applying various, partially empirical, correction approaches.

An important implication for weakly anisotropic materials has so far been disregarded: Intensity contributions due to the sample's crosspolarizing properties can be similar to, or even much lower than, those stemming from polarizer leakage of the copolarizing properties. The mixing of cross- with copolarizing effects can cause pronounced vibrational bandshape and baseline distortions. Polarizer leakage can therefore be detrimental even for qualitative band analyses, rendering

* Corresponding author.
E-mail address: andreas.furchner@helmholtz-berlin.de (A. Furchner).

https://doi.org/10.1016/j.tsf.2022.139560
Received 6 September 2022; Received in revised form 17 October 2022; Accepted 24 October 2022
Available online 29 October 2022
0040-6090/© 2022 The Authors. Published by Elsevier B.V. This is an open access article under the CC BY license (http://creativecommons.org/licenses/by/4.0/).

naive crosspolarized measurements, and interpretation thereof, impossible in such cases. It would thus be highly beneficial to have at hand a measurement scheme and a systematic analysis that provides error-free spectra and that covers both co- and crosspolarized data. Such analysis would not only allow for an accurate description of vibrational bandshapes but also enable the direct interpretation of crosspolarized signals with respect to anisotropic and isotropic contributions.

Indeed, the polarizing properties of imperfect polarizers can be improved by employing sets of tandem polarizers (paired wire-grids) in the incident (polarizer) and detection (analyzer) path [20,22]. However, tandem polarizers naturally exhibit significantly lower transmittances and thus lead to reduced signal-to-noise ratios of the already potentially weak crosspolarized signals. Classical Fourier-transform infrared (FTIR) spectroscopy thin-film sensitive investigations would therefore require significantly longer measurement times.

In this article, we present a convenient measurement scheme for obtaining co- and crosspolarized transmittances (reflectances) using a conventional IR polarimeter equipped with single wire-grid polarizers. This scheme circumvents the need for retrospective spectrum corrections. It makes use of three sample intensity measurements at different parallel and crossed polarizer/analyzer settings. The scheme accounts for first-order leakage effects and is intended to work for polarizer extinction values as small as 100. It also accounts for partial linear source prepolarization typically observed for FTIR spectrometers. Generalizations are possible for measuring signals with integrated polarimetric imaging detectors or polarization-sensitive photodetectors, which are highly relevant for polarimetric imaging applications [25,26].

We apply the scheme to measure the crosspolarized transmission of a weakly anisotropic off-the-shelf polypropylene sheet. The experimental data are evaluated using optical modeling based on anisotropic Lorentzian vibrational oscillators to obtain both sheet thickness and in-plane optical constants in the highly convoluted fingerprint range (1700–780 cm^{-1}) of the material.

2. Measurement scheme

The transmittances $T_{\mathrm{xy}} = |t_{\mathrm{xy}}|^2$ (reflectances $R_{\mathrm{xy}} = |r_{\mathrm{xy}}|^2$), given by the square of the amplitudes of the polarization-dependent complex transmission (reflection) coefficients t_{xy} (r_{xy}), describe the progression of incoming y-polarized light into x-polarized light upon interaction with the sample. For instance, T_{ps} is the crosspolarized transmittance of "s-polarized in, p-polarized out", and T_{ss} is the copolarized transmittance of "s in, s out", where p and s are defined, respectively, as parallel and perpendicular to the polarimeter's plane of incidence.

In an ideal measurement geometry with perfect optical elements, one can acquire the co- and crosspolarized transmittances (reflectances) simply by setting the input polarizer and output analyzer to the corresponding parallel or crossed configuration and referencing the measured intensity to a measurement in a parallel-polarizer configuration without sample. To be concrete, for ideal polarizers, and an unpolarized light source and a polarization-insensitive detector, the co- and crosspolarized transmittances T_{xy} (reflectances R_{xy}) are given by

$$\tilde{T}_{pp} = \frac{I_{0,0}}{J_{0,0}}, \quad \tilde{T}_{sp} = \frac{I_{0,90}}{J_{0,0}}, \quad \tilde{T}_{ps} = \frac{I_{90,0}}{J_{90,90}}, \quad \tilde{T}_{ss} = \frac{I_{90,90}}{J_{90,90}}, \tag{1}$$

where $I_{P,A}$ is the sample intensity measured under polarizer/analyzer azimuths P/A in degrees, and $J_{P,A}$ is the corresponding reference measurement of "air without a sample" used for intensity normalization. In the above nomenclature, a setting of 0° corresponds to p-polarization, whereas 90° refers to s-polarization. The $\sim$ symbol indicates measurements with ideal optical components.

When using an infrared polarimeter with imperfect polarizers, one has to take into account the optical properties of the instrument's individual elements. In particular, the amount of polarizer leakage, described by the polarizer's inverse extinction ratio c, must be considered. Such an analysis is possible within the Mueller calculus [27,28], which describes how an input Stokes vector $\mathrm{S}_{\mathrm{in}} = [s_0, s_1, s_2, s_3]^{\mathrm{T}}$ that characterizes the polarization state of the incoming light is transformed into an output Stokes vector $\mathrm{S}_{\mathrm{out}}$ after interaction with sample and polarimeter + detection optics. For a polarimeter consisting of a polarizer and an analyzer—that is, a set-up geared towards measuring (polarized) transmittances or reflectances—said transformation is given by

$$\mathrm{S}_{\mathrm{out}} = \mathrm{D} \cdot \mathrm{A} \cdot \mathrm{M} \cdot \mathrm{P} \cdot \mathrm{S}_{\mathrm{in}}, \tag{2}$$

where M is the sample's 4 × 4 Mueller matrix, P and A are the polarizer and analyzer matrices (treated as linear diattenuators [27]), and D is the detector matrix. For a polarization-insensitive detector, $\mathrm{D} = \mathrm{diag}(1, 1, 1, 1)$. The infrared source is often an FTIR spectrometer, which tends to exhibit a certain degree of (linear) prepolarization ($s_i/s_0 \neq 0$) originating mainly from the polarizing properties of the FTIR spectrometer's beamsplitter. One therefore usually observes input Stokes vectors of the form $\mathrm{S}_{\mathrm{in}} = [s_0, s_1, 0, 0]^{\mathrm{T}}$ if FTIR and incidence plane of the polarimeter are aligned.

The full treatment of the optical effects of the polarimeter components can be found in Ref. [22]. Under the above assumptions for S_{in} and D, simple expressions can be derived for the inverse polarizer extinction ratio c, the source prepolarization s_1/s_0, and the sample Mueller matrix—the upper-left 2 × 2 block of which can be expressed in terms of the co- and crosspolarized transmittances T_{xy} (reflectances R_{xy}) for a non-depolarizing sample [28].

The polarizer's inverse extinction ratio and the source prepolarization are calculated according to

$$c = \frac{1}{2}\frac{J_{0,90} + J_{90,0}}{J_{0,0} + J_{90,90}}, \quad \frac{s_1}{s_0} = \frac{J_{0,0} - J_{90,90}}{J_{0,0} + J_{90,90}}. \tag{3}$$

c (for a wire-grid polarizer in the fingerprint region) and s_1/s_0 are typically in the promille and percent range, respectively. These values are small but not negligible when measuring crosspolarized signals of weakly anisotropic materials.

For imperfect polarizers, the naive transmittances $\tilde{T}_{\mathrm{xy}}$ from Eq. (1) are related to the sample transmittances T_{xy} as follows:

$$\begin{aligned}
\tilde{T}_{pp} &= T_{pp} + c(T_{sp} + T_{ps}\hat{s}) + c^2(T_{ss} - T_{pp})\hat{s} + \mathcal{O}(c^3)\\
\tilde{T}_{sp} &= T_{sp} + c(T_{pp} + T_{ss}\hat{s}) + c^2(T_{ps} - T_{sp})\hat{s} + \mathcal{O}(c^3)\\
\tilde{T}_{ps} &= T_{ps} + c(T_{ss} + T_{pp}\bar{s}) + c^2(T_{sp} - T_{ps})\bar{s} + \mathcal{O}(c^3)\\
\tilde{T}_{ss} &= T_{ss} + c(T_{ps} + T_{sp}\bar{s}) + c^2(T_{pp} - T_{ss})\bar{s} + \mathcal{O}(c^3)
\end{aligned} \tag{4}$$

Here, source prepolarization comes into play as

$$\bar{s} = \hat{s}^{-1} = \frac{1 + s_1/s_0}{1 - s_1/s_0} = \frac{J_{0,0}}{J_{90,90}}. \tag{5}$$

The above expressions have a simple interpretation: The leading-order terms are the true transmittances T_{xy}. Their measured signals are being modified by contributions of polarizer leakage. At first order [$\mathcal{O}(c)$], either the analyzer is not fully polarizing in the desired direction, or the polarizer is leaking partially orthogonally polarized light onto the sample. The latter effect comes with an additional factor of $\hat{s}$ or $\bar{s}$ because of the sensitivity to source prepolarization at the input side. Second-order effects [$\mathcal{O}(c^2)$], which are modulated when the source radiation is partially polarized, account for a twofold leakage at both the input and the output side. For instance, when measuring $\tilde{T}_{\mathrm{xy}}$, x-prepolarization can leak through the input polarizer, is then converted upon sample interaction into y-polarization, and finally leaks through the output analyzer back into the x-polarization channel.

Eqs. (4) express the naive transmittances $\tilde{T}_{\mathrm{xy}}$ from Eq. (1) in terms of T_{xy} as well as c and s_1/s_0. Conversely, this permits us to invert and solve for T_{xy}. It follows that a minimal set of four sample measurements $I_{P,A}$ and four reference measurements $J_{P,A}$ at distinct parallel and crossed P/A settings is required in order to obtain all co- and crosspolarized

transmittances:

$$\begin{aligned} T_{pp} &= \frac{I_{0,0} - c(I_{0,90} + I_{90,0})}{J_{0,0} + J_{0,90} - c(J_{0,0} + J_{90,90} + J_{0,90} + J_{90,0})} \\ T_{sp} &= \frac{I_{0,90} - c(I_{0,0} + I_{90,90})}{J_{0,0} + J_{0,90} - c(J_{0,0} + J_{90,90} + J_{0,90} + J_{90,0})} \\ T_{ps} &= \frac{I_{90,0} - c(I_{90,90} + I_{0,0})}{J_{90,90} + J_{90,0} - c(J_{0,0} + J_{90,90} + J_{0,90} + J_{90,0})} \\ T_{ss} &= \frac{I_{90,90} - c(I_{90,0} + I_{0,90})}{J_{90,90} + J_{90,0} - c(J_{0,0} + J_{90,90} + J_{0,90} + J_{90,0})} \end{aligned} \quad (6)$$

These formulae account for first-order polarization-leakage effects [$\mathcal{O}(c)$]. Higher-order effects are typically negligible for wire-grid polarizers in the fingerprint region $< 2000\,\mathrm{cm}^{-1}$. The improved formulae for obtaining co- and crosspolarized transmittances or reflectances are suitable for polarizers with extinction ratios as low as about 100, or $c \lesssim 0.01$.

Note that the expressions in Eqs. (4) and (6) are also useful for IR spectroscopists who want to backtrace whether their measurements based on the simplified assumption of ideal polarizers hold true. Provided the appropriate calibration measurements $J_{P,A}$, the original naive measurements from Eq. (1) can be improved in retrospect by calculating $\tilde{T}_{xy}$ according to Eqs. (4) and (6).

It is also noteworthy that the above considerations can be generalized for polarization-sensitive detectors by modifying the matrices $\mathrm{D} \cdot \mathrm{A}$ in the polarization-state analyzer of the polarimeter accordingly. This would allow accurate co- and crosspolarized measurements when employing integrated polarimetric imaging detectors [25] or polarization-sensitive photodetectors [26].

3. Results

We applied the measurement scheme for suppressing unwanted effects from imperfect polarizers to a weakly anisotropic off-the-shelf polypropylene (PP) sheet (Isfort BüroTIPP!, Germany) with a nominal thickness of 33.5 µm. All presented measurements were conducted at normal incidence and at $2\,\mathrm{cm}^{-1}$ spectral resolution using a custom-built infrared polarimeter equipped with a polarization-insensitive photovoltaic mercury–cadmium–telluride detector and single wire-grid polarizers (KRS-5, 0.25 µm wire spacing, Specac Ltd.) as polarizer and analyzer. The set-up was purged with dry air and attached to a Bruker Vertex 70 Fourier-transform spectrometer with a silicon carbide globar as thermal radiation source.

To demonstrate the influence of polarizer leakage on crosspolarized signals, the PP sheet was measured using either the naive approach according to Eq. (1) or the improved scheme of Eq. (6). Prior to the measurements, the sample was azimuthally aligned such that, at 0° rotation, its two in-plane principal axes coincided with the polarimeter's p- and s-polarization directions, as will become apparent later.

Fig. 1 shows typical measurements of crosspolarized transmittances T_{ps} (and $\tilde{T}_{ps}$) in the PP fingerprint region obtained under various azimuthal sample rotations. Film interference fringes emerge in the transparency window above $1500\,\mathrm{cm}^{-1}$. These would not appear in isotropic materials but are present for anisotropic samples as a result of small differences in the in-plane refractive indices (birefringence), making visible even minute differences in the optical thicknesses $n_x \times d$ and $n_y \times d$. A highly convoluted collection of anisotropic vibrational bands is seen below $1500\,\mathrm{cm}^{-1}$.

Fig. 1 (top) showcases T_{ps} spectra obtained at maximal and minimal crosspolarization, that is, under 45°/135° and 0°/90° azimuthal sample rotation. Baselines of zero are expected in spectral regions without anisotropic contributions. This is observed only in a few places in the absorbing range because virtually every PP vibrational band exhibits some degree of anisotropy. However, T_{ps} is zero over the entire spectral range for 0° and 90° sample orientation. In these positions, the two in-plane principal axes are aligned with the polarimeter's coordinate

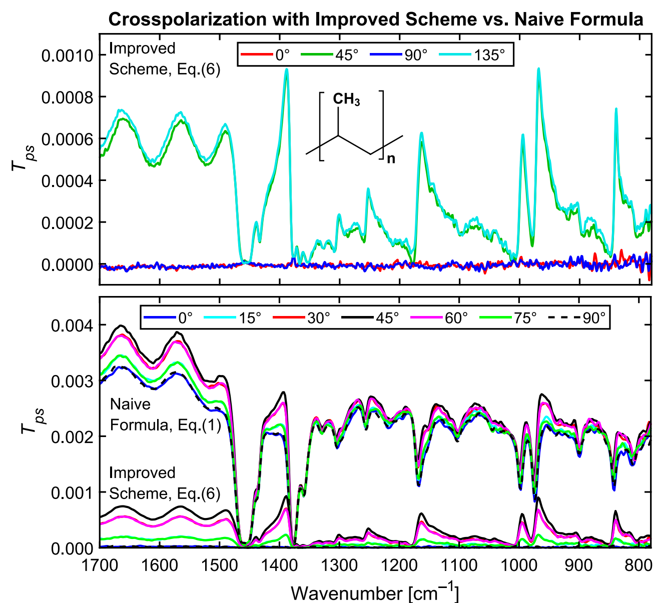

Fig. 1. Crosspolarized transmittance T_{ps} of a weakly in-plane anisotropic polypropylene sheet measured under different azimuthal sample rotations. Transmittances were calculated assuming either ideal polarizers ($\tilde{T}_{ps}$) after Eq. (1) or imperfect polarizers (T_{ps}) after Eq. (6). Top: Measurements at minimal and maximal crosspolarization (0°, 90°; 45°, 135° azimuth). Bottom: Measurements between 0° (p-polarized orientation) and 90° (s-polarized orientation).

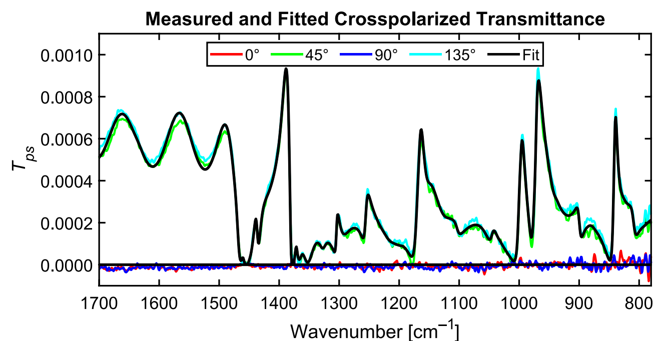

Fig. 2. Measured and fitted crosspolarized transmittance T_{ps} of the anisotropic polypropylene sheet, shown at selected sample azimuths of minimal and maximal crosspolarization.

system, resulting in pseudo-isotropic optical responses. Measurements under 45° and 135° sample orientation are expected to yield the strongest crosspolarized signals. With T_{ps} values smaller than 0.001, the polymer sheet's in-plane anisotropy is apparently rather weak.

Fig. 1 (bottom) depicts how T_{ps} measured with the improved scheme compares with the naively obtained $\tilde{T}_{ps}$ under varying sample azimuths between 0° and 90°. Pronounced bandshape and baseline distortions are observed in $\tilde{T}_{ps}$. In fact, $\tilde{T}_{ps}$ never drops below 0.001 for wavenumbers $< 1350\,\mathrm{cm}^{-1}$. Predictably, this value is close to the wire-grid polarizer's inverse extinction of $c \approx 0.001 \ldots 0.002$ in the presented spectral range. Furthermore, the bandshapes are strongly distorted, rendering a direct quantitative, or even qualitative, analysis impossible. In stark contrast, the improved scheme for obtaining T_{ps} leads to correct bandshapes and baselines, thus enabling qualitative and quantitative interpretations with regard to weak anisotropy.

Intermediate values between zero and maximum crosspolarization are found for the remaining angles. For symmetry reasons of the material's dielectric tensor, the respective measurements at $45° \pm \theta$ are identical.

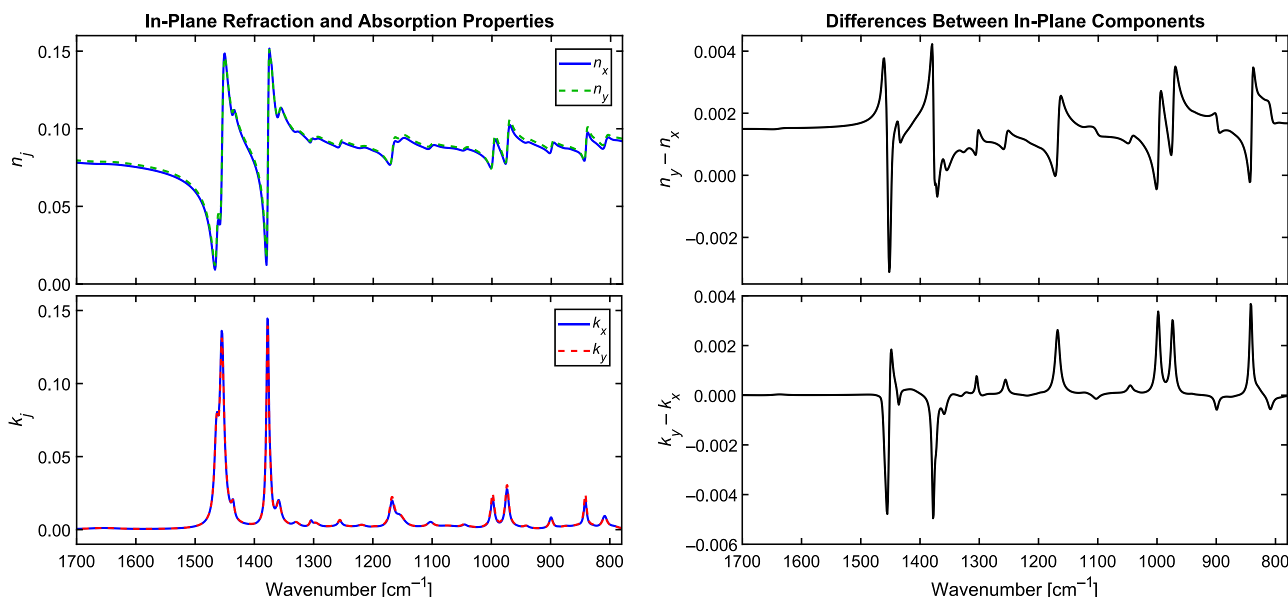

Fig. 3. Fitted absolute values (left) of, and differences (right) between, the in-plane refraction (n_j, top) and absorption (k_j, bottom) properties of the anisotropic polypropylene sheet.

This symmetry is seen in the naively calculated transmittances, too. However, because the much stronger leaking copolarized signals mask the crosspolarized signals of interest, a quantitative band analysis and identification of isotropic and anisotropic effects are not possible for $\tilde{T}_{xy}$. In fact, from such naive measurements without the inclusion of c-terms in Eq. (4), one could wrongly deduce that the sample exhibits more complex anisotropic properties than it actually does.

Interestingly, with Eq. (4) and post-hoc knowledge of the sample's in-plane principal axes, one can understand the observed band intensities in the naive crosspolarized transmittances. Due to polarizer leakage, maximum band amplitudes in $\tilde{T}_{ps}$ are found at 0° and 90° sample orientation where the copolarized transmittances, and hence the leaking signals, are maximal.

Having at hand accurate crosspolarization data of the weakly anisotropic polymer sheet is a prerequisite for the quantitative interpretation of the material's optical response. We now apply conventional optical modeling techniques to quantify the in-plane components (x and y) of the polypropylene sheet's anisotropic complex dielectric tensor

$$\varepsilon = \begin{bmatrix} \varepsilon_x & 0 & 0 \\ 0 & \varepsilon_y & 0 \\ 0 & 0 & \varepsilon_z \end{bmatrix} = \begin{bmatrix} (n_x + ik_x)^2 & 0 & 0 \\ 0 & (n_y + ik_y)^2 & 0 \\ 0 & 0 & (n_z + ik_z)^2 \end{bmatrix}, \quad (7)$$

i. e., the in-plane refraction (n_j) and absorption (k_j) properties. The azimuth-dependent complex transmittances were calculated by employing a 4×4 transfer-matrix algorithm [29] for a simple anisotropic layer model consisting of "Air / PP Sheet / Air". The dielectric function

$$\varepsilon_j(\tilde{\nu}) = \varepsilon_\infty^{(j)} + \sum_n \varepsilon_{n,\mathrm{vib}}^{(j)}(\tilde{\nu}), \quad j = x, y, z \quad (8)$$

of PP was composed of anisotropic Lorentzian-shaped vibrational oscillators $\varepsilon_{n,\mathrm{vib}}^{(j)}$, which describe the numerous vibrational absorption bands, plus a direction-dependent high-frequency dielectric constant $\varepsilon_\infty^{(j)}$, which accounts for birefringence from electronic and other vibrational transitions that occur at higher energies outside the considered spectral range [30,31]. In order to minimize the number of fit parameters and the correlation between them, oscillator positions and widths were kept the same in x and y direction, whereas oscillator amplitudes were allowed to vary.

The dielectric tensor and the orientation of the PP sheet's principal axes were fitted by applying a standard χ^2 minimization [30] between theoretical and measured multi-azimuth data. Additionally, the PP thickness d was fitted, including a small linear thickness gradient (320 nm) within the measurement spot due to inhomogeneities of the polymer sheet. Results are shown in Fig. 2 for measured and calculated T_{ps} at selected azimuths of minimal and maximal crosspolarization (0°, 90°; 45°, 135°). Both the transparent region above and the absorbing region below 1500 cm^{-1} are well-described by the model.

The weak T_{ps} signatures of less than 0.001 already imply a rather weak anisotropy of the PP sheet. Indeed similarly small are the differences between the fitted components of the complex refractive indices of the two in-plane directions ($n_y - n_x$ and $k_y - k_x$), as depicted in Fig. 3. These differences are in fact barely noticeable at the level of the absolute n_j and k_j data (also shown in Fig. 3).

A detailed discussion of the rich vibrational fingerprint of PP is beyond the scope of this article. However, the observed different bandshapes already point toward differing orientations of the related transition dipole moments.

The above quantification of the PP sheet's anisotropic dielectric tensor hinges on the accurate measurement of crosspolarized polarimetric data. Our improved scheme for acquiring co- and crosspolarized transmittances (reflectances) accounts for both polarizer leakage and potential source polarization. The scheme has thus enabled detailed quantitative insights into the vibrational bands of this weakly anisotropic polymer sample.

4. Conclusions and outlook

Polarizer leakage causes bandshape and baseline distortions in crosspolarized polarimetric measurements. These disturbances can be so strong that direct spectra interpretations with respect to isotropy and anisotropy of the studied material become unfeasible. A polarimetric measurement scheme for handling the errors due to polarizer leakage and source prepolarization was proposed and proven to be applicable for the band analysis of crosspolarized spectra of weakly anisotropic polypropylene sheets. Corresponding measurement schemes will be deduced for the analysis of generalized ellipsometric amplitude and phase parameters. This work is of particular relevance for IR-polarimetric investigations of anisotropic functional thin films but also for *in situ* and *operando* studies of anisotropic processes such as film growth or reactions at catalytic surfaces.

CRediT authorship contribution statement

Andreas Furchner: Conceptualization, Methodology of IR measurements, IR investigation, Data evaluation, Writing – original draft & editing, Visualization. **Karsten Hinrichs:** Conceptualization, IR investigation, Data evaluation, Resources, Writing – review.

Declaration of competing interest

The authors declare that they have no known competing financial interests or personal relationships that could have appeared to influence the work reported in this paper.

Data availability

Data underlying the results presented in this paper are not publicly available at this time but may be obtained from the authors upon reasonable request.

Acknowledgments and funding

Application Lab for Infrared Ellipsometry via the Europäischer Fonds für regionale Entwicklung (EFRE, 1.8/13); Ministerium für Kultur und Wissenschaft des Landes Nordrhein-Westfalen; Die Regierende Bürgermeisterin von Berlin – Senatsverwaltung Wissenschaft, Gesundheit, Pflege und Gleichstellung; Bundesministerium für Bildung und Forschung. The authors acknowledge support from the Federal Ministry of Education and Research, Germany in the framework of the project CatLab (03EW0015A/B).

References

[1] P. Winkler, J. Zeininger, Y. Suchorski, M. Stöger-Pollach, P. Zeller, M. Amati, L. Gregoratti, G. Rupprechter, How the anisotropy of surface oxide formation influences the transient activity of a surface reaction, Nature Commun. 12 (1) (2021) 69, http://dx.doi.org/10.1038/s41467-020-20377-9.

[2] K. Song, J. Jung, M. Park, H. Park, H.-J. Kim, S.-I. Choi, J. Yang, K. Kang, Y.-K. Han, Y.-M. Kang, Anisotropic Surface Modulation of Pt Catalysts for Highly Reversible Li–O2 Batteries: High Index Facet as a Critical Descriptor, ACS Catal. 8 (10) (2018) 9006–9015, http://dx.doi.org/10.1021/acscatal.8b02172.

[3] K. Hinrichs, T. Shaykhutdinov, Polarization-Dependent Atomic Force Microscopy–Infrared Spectroscopy (AFM-IR): Infrared Nanopolarimetric Analysis of Structure and Anisotropy of Thin Films and Surfaces, Appl. Spectroscopy 72 (6) (2018) 817–832, http://dx.doi.org/10.1177/0003702818763604.

[4] Q. Zhang, L.A. Archer, Optical Polarimetry and Mechanical Rheometry of Poly(ethylene oxide)–Silica Dispersions, Macromolecules 37 (5) (2004) 1928–1936, http://dx.doi.org/10.1021/ma035667v.

[5] M. Benelajla, E. Kammann, B. Urbaszek, K. Karrai, Physical Origins of Extreme Cross-Polarization Extinction in Confocal Microscopy, Phys. Rev. X 11 (2) (2021) 021007, http://dx.doi.org/10.1103/PhysRevX.11.021007.

[6] J.M. Schmitt, S.H. Xiang, Cross-polarized backscatter in optical coherence tomography of biological tissue, Opt. Lett. 23 (13) (1998) 1060–1062, http://dx.doi.org/10.1364/OL.23.001060.

[7] R.V. Kuranov, V.V. Sapozhnikova, I.V. Turchin, E.V. Zagainova, V.M. Gelikonov, V.A. Kamensky, L.B. Snopova, N.N. Prodanetz, Complementary use of cross-polarization and standard OCT for differential diagnosis of pathological tissues, Opt. Express 10 (15) (2002) 707–713, http://dx.doi.org/10.1364/OE.10.000707.

[8] M. Pircher, C.K. Hitzenberger, U. Schmidt-Erfurth, Polarization sensitive optical coherence tomography in the human eye, Progr. Retinal Eye Res. 30 (6) (2011) 431–451, http://dx.doi.org/10.1016/j.preteyeres.2011.06.003.

[9] M.D. Higgins, Imaging birefringent minerals without extinction using circularly polarized light, Can. Mineral. 48 (1) (2010) 231–235, http://dx.doi.org/10.3749/canmin.48.1.231.

[10] M. Esslinger, J. Dorfmüller, W. Khunsin, R. Vogelgesang, K. Kern, Background-free imaging of plasmonic structures with cross-polarized apertureless scanning near-field optical microscopy, Rev. Sci. Instrum. 83 (3) (2012) 033704, http://dx.doi.org/10.1063/1.3693346.

[11] K. Chen, D. Fried, Multispectral cross-polarization reflectance measurements suggest high contrast of demineralization on tooth surfaces at wavelengths beyond 1300 nm due to reduced light scattering in sound enamel, J. Biomed. Opt. 23 (6) (2018) 060501, http://dx.doi.org/10.1117/1.JBO.23.6.060501.

[12] K. Hinrichs, B. Blevins, A. Furchner, N.S. Yadavalli, S. Minko, Infrared polarimetry: Anisotropy of polymer nanofibers, Micro Nano Eng. 14 (2022) 100116, http://dx.doi.org/10.1016/j.mne.2022.100116.

[13] Y. Miyauchi, M. Oba, S. Maruyama, Cross-polarized optical absorption of single-walled nanotubes by polarized photoluminescence excitation spectroscopy, Phys. Rev. B 74 (20) (2010) 205440, http://dx.doi.org/10.1103/PhysRevB.74.205440.

[14] P. Gordon, V.P. Venancio, S.U. Mertens-Talcott, G.L. Coté, Portable bright-field, fluorescence, and cross-polarized microscope toward point-of-care imaging diagnostics, J. Biomed. Opt. 24 (9) (2019) 096502, http://dx.doi.org/10.1117/1.JBO.24.9.096502.

[15] S.I. Bozhevolnyi, M. Xiao, O. Keller, External-reflection near-field optical microscope with cross-polarized detection, Appl. Opt. 33 (5) (1994) 876–880, http://dx.doi.org/10.1364/AO.33.000876.

[16] T.W.H. Oates, B. Dastmalchi, C. Helgert, L. Reissmann, U. Huebner, E.-B. Kley, M.A. Verschuuren, I. Bergmair, T. Pertsch, K. Hingerl, K. Hinrichs, Optical activity in sub-wavelength metallic grids and fishnet metamaterials in the conical mount, Opt. Mater. Express 3 (4) (2013) 439–451, http://dx.doi.org/10.1364/OME.3.000439.

[17] A. Ishikawa, S. Hara, T. Tanaka, Y. Hayashi, K. Tsuruta, Cross-Polarized Surface-Enhanced Infrared Spectroscopy by Fano-Resonant Asymmetric Metamaterials, Sci. Rep. 7 (2017) 3205, http://dx.doi.org/10.1038/s41598-017-03545-8.

[18] K. Järrendahl, H. Arwin, Polarizing Natural Nanostructures, in: K. Hinrichs, K.-J. Eichhorn (Eds.), Ellipsometry of Functional Organic Surfaces and Films, Springer Series in Surface Sciences, vol 52. Springer, ISBN: 978-3-319-75894-7, 2018, http://dx.doi.org/10.1007/978-3-319-75895-4_11.

[19] K.B. Rodenhausen, D. Schmidt, C. Rice, T. Hofmann, E. Schubert, M. Schubert, Detection of Organic Attachment onto Highly Ordered Three-Dimensional Nanostructure Thin Films by Generalized Ellipsometry and Quartz Crystal Microbalance with Dissipation Techniques, in: K. Hinrichs, K.-J. Eichhorn (Eds.), Ellipsometry of Functional Organic Surfaces and Films, Springer Series in Surface Sciences, vol 52. Springer, ISBN: 978-3-319-75894-7, 2018, http://dx.doi.org/10.1007/978-3-319-75895-4_10.

[20] J.-C. Cigal, A Novel Spectroscopic Ellipsometer in the Infrared (Ph.D. thesis), Technische Universiteit Eindhoven, Eindhoven, The Netherlands, ISBN: 90-386-1555-8, 2002, http://dx.doi.org/10.6100/IR559797, URL https://research.tue.nl/en/publications/a-novel-spectroscopic-ellipsometer-in-the-infrared.

[21] J. Bremer, O. Hunderi, K. Fanping, T. Skauli, E. Wold, Infrared ellipsometer for the study of surfaces, thin films, and superlattices, Appl. Opt. 31 (4) (1992) 471–478, http://dx.doi.org/10.1364/AO.31.000471.

[22] A. Furchner, C. Walder, M. Zellmeier, J. Rappich, K. Hinrichs, Broadband infrared Mueller-matrix ellipsometry for studies of structured surfaces and thin films, Appl. Opt. 57 (27) (2018) 7895–7904, http://dx.doi.org/10.1364/AO.57.007895.

[23] V.P. Tolstoy, I.V. Chernyshova, V.A. Skryshevsky, Handbook of Infrared Spectroscopy of Ultrathin Films, John Wiley & Sons, Inc., Chichester, ISBN: 978-0-471-23432-6, 2003, http://dx.doi.org/10.1002/047123432X.ch1.

[24] D. Blaudez, T. Buffeteau, B. Desbat, P. Fournier, A.-M. Ritcey, M. Pézolet, Infrared Reflection–Absorption Spectroscopy of Thin Organic Films on Nonmetallic Substrates: Optimal Angle of Incidence, J. Phys.. Chem. B 102 (1) (1998) 99–105, http://dx.doi.org/10.1021/jp9710188.

[25] Q. Li, Z. Li, N. Li, X. Chen, P. Chen, X. Shen, W. Lu, High-Polarization-Discriminating Infrared Detection Using a Single Quantum Well Sandwiched in Plasmonic Micro-Cavity, Sci. Rep. 4 (2014) 6332, http://dx.doi.org/10.1038/srep06332.

[26] J. Wang, C. Jiang, W. Li, X. Xiao, Anisotropic Low-Dimensional Materials for Polarization-Sensitive Photodetectors: From Materials to Devices, Adv. Opt. Mater. 10 (6) (2022) 2102436, http://dx.doi.org/10.1002/adom.202102436.

[27] R.A. Chipman, Polarimetry, in: M. Bass (Ed.), Handbook of Optics, McGraw Hill, New York, ISBN: 0-07-047974-7, 1995.

[28] J.J. Gil Pérez, R. Ossikovski, Polarized Light and the Mueller Matrix Approach, CRC Press, ISBN: 978-1-482-25155-5, 2016, http://dx.doi.org/10.1201/b19711.

[29] M. Schubert, Polarization-dependent optical parameters of arbitrarily anisotropic homogeneous layered systems, Phys. Rev. B 53 (8) (1996) 4265–4274, http://dx.doi.org/10.1103/PhysRevB.53.4265.

[30] H.G. Tompkins, E.A. Irene, Handbook of Ellipsometry, William Andrew, Inc., Norwich, ISBN: 978-0-8155-1499-2, 2005, URL http://www.sciencedirect.com/science/book/9780815514992.

[31] K. Hinrichs, K.-J. Eichhorn, Ellipsometry of Functional Organic Surfaces and Films, Springer-Verlag Berlin Heidelberg, ISBN: 978-3-319-75894-7, 2018, http://dx.doi.org/10.1007/978-3-319-75895-4.